OPEN

PRS GLOBAL OPEN

ORIGINAL ARTICLE
Research

Preservation of Eschar Prevents Excessive Wound Healing by Reducing M2 Macrophages Polarization

Mingyue Shi, MD
Yao Lu, MD
Ali Mohyeddin, PhD
Fazhi Qi, MD
Yuyan Pan, MD

Background: Removal of the eschar has gradually become a consensus on treatments of deep dermal necrosis after skin trauma in recent years, whereas exaggerated scar contracture and tissue proliferation developed during healing have received little attention. Here, the authors investigated the effects of eschar on excessive wound healing of small dermal damage and focused on the role M2 macrophages played, hoping to offer a theoretical basis to improve patients' cosmetic satisfaction.

Methods: A mouse dorsal wound model (n = 12) was established by electric heating pads heating for 20 seconds on each side of the spine, and the left side was the preserved group. Macrophage numbers, expression of wound-healing-associated proteins, and inflammatory cytokine levels were assessed at different time points by immunohistochemistry and quantitative real-time polymerase chain reaction. A co-culture system of M2 macrophages and myofibroblasts was created in vitro. Immunohistochemistry, real-time polymerase chain reaction, and Western blot were performed to evaluate the proliferation, migration, and protein expression of myofibroblasts.

Results: Preserving eschar inhibited contraction-associated proteins (α-smooth muscle actin and vimentin) and collagen expression, inflammatory cytokine (IL-1β, IL-10, TFN-α, and IL-4) expression, and M2 macrophage infiltration. Mechanistically, M2 macrophages potentially contributed to excessive wound healing by promoting myofibroblasts proliferation, migration, and production of contraction-associated proteins.

Conclusion: Eschar preservation in wounds could reduce inflammation and negatively modulate myofibroblasts by inhibiting M2 macrophage polarization and infiltration, preventing excessive wound contraction and collagen deposition. *(Plast Reconstr Surg Glob Open 2023; 11:e5238; doi: 10.1097/GOX.0000000000005238; Published online 18 September 2023.)*

INTRODUCTION

Cosmetic procedures have gained popularity in the last decades,[1] showing a nearly 10% increase in 2021 from the previous year. However, with the growing demand for cosmetic surgery, cases developing complications increase correspondingly. The Food and Drug Administration reported that over 2800 injection-related discomfort occurred in the United States from 2013 to 2017.[2] Skin necrosis is one of the most adverse events.[3] Generally, irregular or burn-like erythema covered with fluid-filled blisters is seen on the wound, followed by exudation of serous fluid forming crust and finally becoming a dry, thick, leathery tissue.

Skin necrosis after cosmetic surgery is similar to the dead tissue and secretions caused by deep-degree burns, which can be broadly defined as eschar. The treatment in this situation often directly draws on the experience of extensive burn injury treatments. Escharectomy followed by substitution with a skin graft is a conventional treatment[4] for patients with extensive deep burn injury, beneficial for lower infection rate[5] and less inflammation. Other clinical approaches to the debridement of burn

From the Department of Plastic Surgery, Zhongshan Hospital, Fudan University, Shanghai, China.

Received for publication March 1, 2023; accepted July 11, 2023.

Drs. Mingyue Shi and Yao Lu, and Drs. Yuyan Pan and Fazhi Qi contributed equally to this work.

DOI: 10.1097/GOX.0000000000005238

Disclosure statements are at the end of this article, following the correspondence information.

Related Digital Media are available in the full-text version of the article on www.PRSGlobalOpen.com.

wounds are numerous, including wound excision, enzymatic debridement,[6] hydrosurgery, larvae therapy,[7] and debridement by laser.[8] However, the skin necrosis area after cosmetic procedures is relatively smaller and more cleaned, which may lead to a different environment[9] and capabilities of cells[10] in the wound periphery with a lower risk of infection. Therefore, treatments of skin necrosis in cosmetic surgery should not be completely similar to burns, which has still not been explored theoretically.[11] A study reported the inhibitory effect of burn wound extract on endothelial proliferation,[12] and other studies demonstrated that when eschar is only partially removed,[13] the formation of hypertrophic, retraction, and painful scars[14] could be avoided, but clinical evidence and theoretical basis to support its efficacy are still lacking.

Scar formation is considered abnormal when excessive fibrosis and inflammation are critical steps in wound healing.[15] Several studies have found that excessive type 1 immunity causes tissue damage and necrosis, whereas excessive type 2 immunity results in fibrosis,[16] related to inflammatory cytokines and immune cells.[17] Unlike M1 macrophages, mainly involved in granulation tissue formation and re-epithelialization in the early phase, M2 macrophages, acting as an anti-inflammatory, favor tissue repair and scar formation in the later phase.[18] As is well known, M2 macrophages induce the proliferation and differentiation of fibroblasts into myofibroblasts. Studies demonstrated that myofibroblasts are necessary for excessive collagen formation and alpha-smooth muscle (α-SMA) expression in aberrant scars.[19] Thus, there is some speculation that excess polarization of M2 macrophages could promote pathological fibrosis and aberrant repair, which has already been validated in renal interstitial fibrosis[20] and idiopathic pulmonary fibrosis.[21] Still, the relationship between M2 and myofibroblasts has not been confirmed in eschar.

Taken together, we assume that eschar preservation suppresses excessive fibrosis and scar formation in the later phase of wound healing, dominated by decreasing M2 macrophages and accompanied by a coordinated decline in myofibroblasts, which provides a rationale for improving aesthetic healing of small but deep wounds in clinical use.

Takeaways

Question: Removal of the eschar has gradually become a consensus on treatments of deep dermal necrosis after skin trauma in recent years, whereas exaggerated scar contracture and tissue proliferation developed during healing have received little attention, which is what we studied.

Findings: We found the eschar preservation in wounds could reduce inflammation and negatively modulate myofibroblasts by inhibiting M2 macrophage polarization and infiltration, preventing excessive wound contraction and collagen deposition.

Meaning: For small but deep wounds, our study revealed appropriate preserving eschar prevented excessive wound healing after dermal necrosis, which offered a theoretical basis for the benefit of better aesthetic wound healing.

MATERIALS AND METHODS

Animal Experiments

C57BL/6 mice (age 6-8 weeks; weight, 20-25g; males) were obtained from the Shanghai SLAC Laboratory Animal Co., Ltd. (China). All treatments and experimental procedures were approved by the Animal Ethics Committee of Zhongshan Hospital (Fudan University, Shanghai, China).

The mice (n = 12) were anesthetized by intraperitoneal injection of 10% chloral hydrate (3 mL/kg). Dorsal fur was removed and the skin was disinfected with 75% alcohol. Three cutaneous burn injuries (diameter 9 mm) were made on each side of the spine on the mice's dorsal skin by exposure to electric heating pads at around 100°C for 20 seconds. The wounds were covered with cotton balls moistened with sterile 0.9% saline solution after being disinfected and immobilized by transparent dressing.

The dorsal injuries of each mouse were divided into two groups: the wound on the left side of the spine was the preserved group, and the wound on the right side of the spine was the removal group (**See figure, Supplemental Digital Content 1,** which shows three wounds on each side of the mouse dorsal skin, covered with cotton balls and transparent dressing. **http://links.lww.com/GOX/A0**). Mice were anesthetized and disinfected 24 hours after the wound was created, and dense tissue of the necrotic skin on the right side of the spine was removed until the loose part was exposed, approximately to the deep dermis. Each mouse's tissue was harvested on 2, 5, 8, 14, and 21 days after surgery for analysis.

Immunohistochemistry

Tissue samples were fixed in 4% paraformaldehyde (Biosharp, Wuhan, China) for 48 hours and then dehydrated, embedded in paraffin (Guangdong Dachuan special wax Co. Ltd, Guangdong, China), and serially sectioned (at a thickness of 5-μm) for hematoxylin and eosin (HE) staining (Ribiology, Shanghai, China) and Masson trichrome staining (Besso, Zhuhai, China).

Sections were incubated with primary antibodies against CD68, CD206, α-SMA, and vimentin at 4°C overnight. After the reaction with secondary antibodies at room temperature for 1 hour, visualization was achieved using diaminobenzidine. Nuclei were counterstained with hematoxylin (**See table, Supplemental Digital Content 2,** which shows antibodies used in this experiment. **http://links.lww.com/GOX/A1**).

Real-time Quantitative Polymerized Chain Reaction

Total RNA was extracted from tissues or cells. After reverse transcription, real-time quantitative polymerized chain reaction (RT-PCR) was performed using qPCR SYBR Green Master Mix. We chose α-SMA, vimentin, fibronectin, and inflammatory factors as targets. Relative gene expression was measured by the $2^{-\triangle\triangle CT}$ methods, with

GAPDH as the internal control. (**See table, Supplemental Digital Content 3,** which shows primer sequences for RT-PCR used in this experiment. **http://links.lww.com/GOX/A2**.)

Culture

Human foreskin fibroblasts (HFF-1) were cultured in Dulbecco modified Eagle medium without fetal bovine serum (FBS; Gibco, USA) for 12 hours, and then the culture medium was replaced by high glucose Dulbecco modified Eagle medium with 10% FBS. Fibroblast differentiation into myofibroblast was induced with TGF-β1 (10 ng/mL) for 48 hours. Human myeloid leukemia mononuclear cells (THP-1) were cultured in 1640 Medium containing 10% FBS, differentiated into macrophages by a 48-hour incubation with 50 ng/mL phorbol 12-myristate 13-acetate (Abcam, Shanghai, China). Macrophages were polarized to M2 macrophages by adding 20 ng per mL IL-4 and IL-13 to the media for an additional 48 hours.

The Transwell co-culture assay was performed using the six-well transwell plates (Labselect, Shanghai, China). Myofibroblasts were applied to the lower compartment, whereas M2 macrophages were added to the upper compartment of the plates.

Scratch Assay

Scratch experiments were used to investigate cell migration behavior. HFF-1s (1.5×10^6 cells) at log-phase growth were seeded in six-well plates and induced into myofibroblasts. A scratch model was prepared by a cross-shaped scratch made on the cell monolayer with the tip of a sterile 200 μL pipette, with PBS used to wash off any exfoliated cells. Images of the samples were taken and recorded after 6, 12, 24 hours of treatment, and the cell migration area was calculated and compared using Image J software (NIH software, America).

Cell Counting Kit-8 Assay

Cell proliferation was measured using Cell Counting Kit-8 (CCK-8) assay (Hanheng, Shanghai, China). Cells were seeded in a 96-well plate at a density of 2000 cells per well. After being cultured for 12 hours, the previous medium was discarded, and 50 μL 24, 48-hour supernatant of M0/M2 macrophages combined with 50 μL complete medium were added to each well. The medium was replaced with 10 μL CCK-8 solution and 90 μL RPMI 1640 cell culture medium after 0/12/24/48 hour treatment of supernatant. The optical density value was measured by spectrophotometer (Denovix, Wilmington, USA) at 450 nm after 1.5 hour in the incubator.

Western Blot

Total protein harvested from tissues was separated by 10% SDS-PAGE and blotted onto nitrocellulose membrane (Millipore, Shanghai, China), incubated with the diluted primary antibodies overnight at 4°C. Subsequently, the membrane was incubated with secondary antibodies for 1 hour at room temperature, and blot images were captured by chemiluminescence image analysis system (Tianneng, Beijing, China). GAPDH expression was used as the internal control.

Statistical Analysis

Statistics were calculated using BM SPSS Statistics 20 (IBM Corp., N.Y.), and statistical graphs were drawn using GraphPad Prism 9. The *t* test analyzed the differences between the two groups. One-way ANOVA performed comparisons of multiple groups. All values were expressed as mean ± SD, and a value of *P* less than 0.05 was considered to be statistically significant.

RESULTS

Construction of the Wound Eschar Model

Compared with normal mouse skin, the skin after heating for 20 seconds was obviously degenerated, with thinning of the epidermis and compaction of the collagen in the deep dermis (Fig. 1). Image J software showed the depth of skin necrosis was (503.26 ± 24.38) μm, which was as deep as the dermal layer. Thus, the mouse dorsal skin heated for 20 seconds was chosen for subsequent experiments.

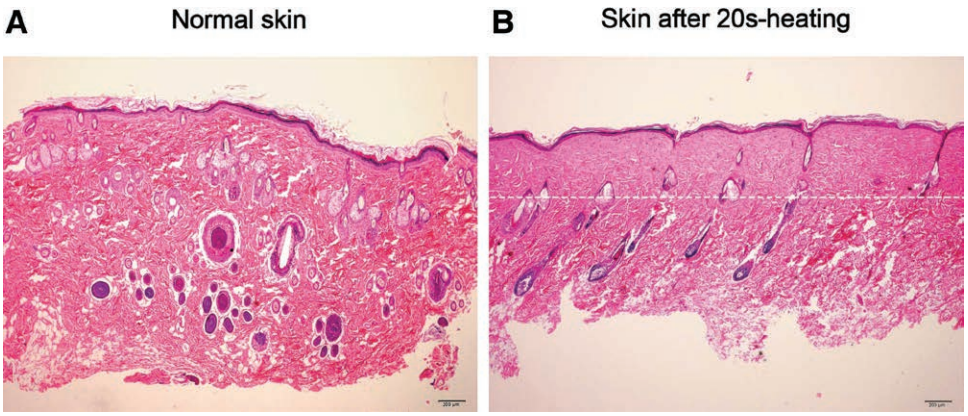

Fig. 1. Histology of the wound eschar in mice. HE staining of normal mouse skin (A) and mouse skin after heating for 20 seconds with the heating pads (B). HE staining, hematoxylin-eosin staining.

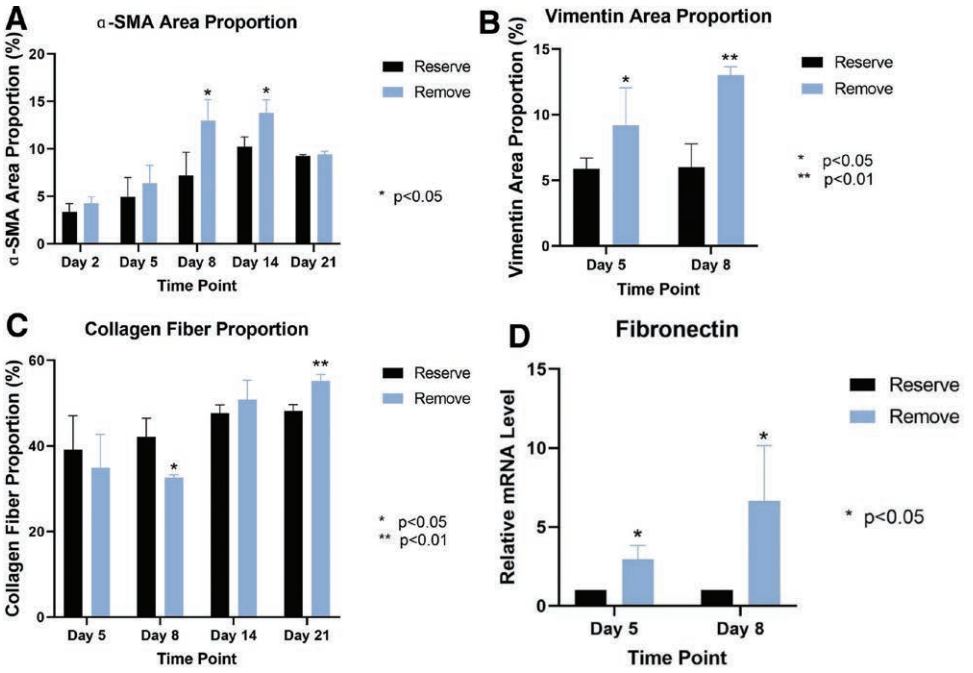

Fig. 2. Reserving eschar reduced expression of wound-healing-associated proteins. α-SMA/vimentin (A, B) and collagen fiber (C) were monitored by IHC and quantified by ImageJ software. The mRNA gene expression of fibronectin (D). Data are presented as mean ± S.D.; **P* < 0.05, ***P* < 0.01, as compared with the preserved group each day. α-SMA, α-smooth muscle actin; IHC, immunohistochemistry.

Preserving Eschar Inhibited Excessive Wound Contraction and Collagen Deposition

As important proteins contributing to wound contraction, the expression of α-SMA was evidently upregulated by the removal of eschar on day 8 (n = 12, 12.99 ± 1.80% versus 7.23 ± 1.97%, $P < 0.05$) and day 14 (n = 12, 13.83 ± 1.09% versus 10.22 ± 0.87%, $P < 0.05$). Vimentin-positive areas after removal were also more than the retention group on day 5 (n = 12, 9.19 ± 2.56% versus 5.88 ± 0.74%, $P < 0.05$) and day 8 (n = 12, 13.02 ± 0.51% versus 5.99 ± 1.46%, $P < 0.01$) (Fig. 2A, B) (**See figure, Supplemental Digital Content 4,** which demonstrates IHC staining of α-SMA and vimentin in the removal and the preserved group. **http://links.lww.com/GOX/A3**). (**See figure, Supplemental Digital Content 5,** which demonstrates IHC staining of α-SMA and vimentin in the removal and the preserved group. **http://links.lww.com/GOX/A4**)

Consistent with contraction-associated proteins, the mRNA level of fibronectin (Fig. 2C) of the removal group was strikingly enhanced compared to that in the preserved group on day 5 (n = 12, 2.97 ± 0.70 times, $P < 0.05$) and day 8 (n = 12, 6.66 ± 2.85 times, $P < 0.05$). While the proportion of collagen (Fig. 2D) in the full-thickness skin with debridement decreased first and then showed an increasing trend over time, it was significantly higher than the other group on day 21 (n = 12, 55.25 ± 1.19% versus 48.24 ± 1.19%, $P < 0.01$). (**See figure, Supplemental Digital Content 6,** which demonstrates IHC staining of collagen fiber in the removal and the preserved group. **http://links.lww.com/GOX/A5**.)

Reserving Eschar Declined the Excessive Inflammatory Responses

The results of RT-PCR indicated that eschar preservation markedly attenuated the expression of inflammatory factors (Fig. 3) on day 5, including IL-1β (n = 12, 3.50 ± 1.76 times, $P < 0.05$), IL-10 (n = 12, 5.18 ± 1.79 times, $P < 0.01$) and TNF-α (n = 12, 3.28 ± 1.16 times, $P < 0.05$). Interestingly, IL-4 had a higher concentration in the removal group on day 2 (n = 12, 8.43 ± 1.98 times, $P < 0.001$), but became lower than the preserved group

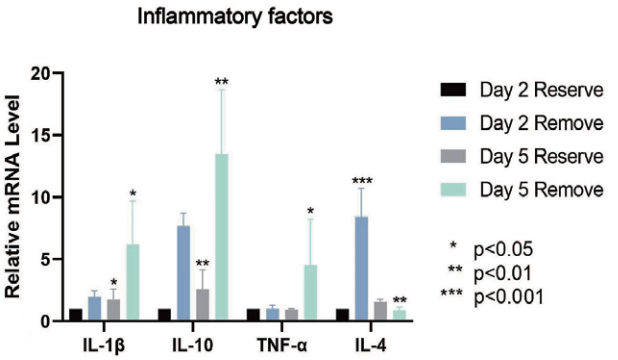

Fig. 3. Reserving eschar downregulated the gene expression of inflammatory factors IL-6, IL-10, TNF-α, and IL-4. The mRNA level of inflammatory factors in the preserved group on day 2 was set as 1, and the relative mRNA levels of different groups at different times were compared. Data are presented as mean ± S.D.; **P* < 0.05, ***P* < 0.01, ****P* < 0.001, as compared with the preserved group each day. IL, interleukin; TNF, tumor necrosis factor.

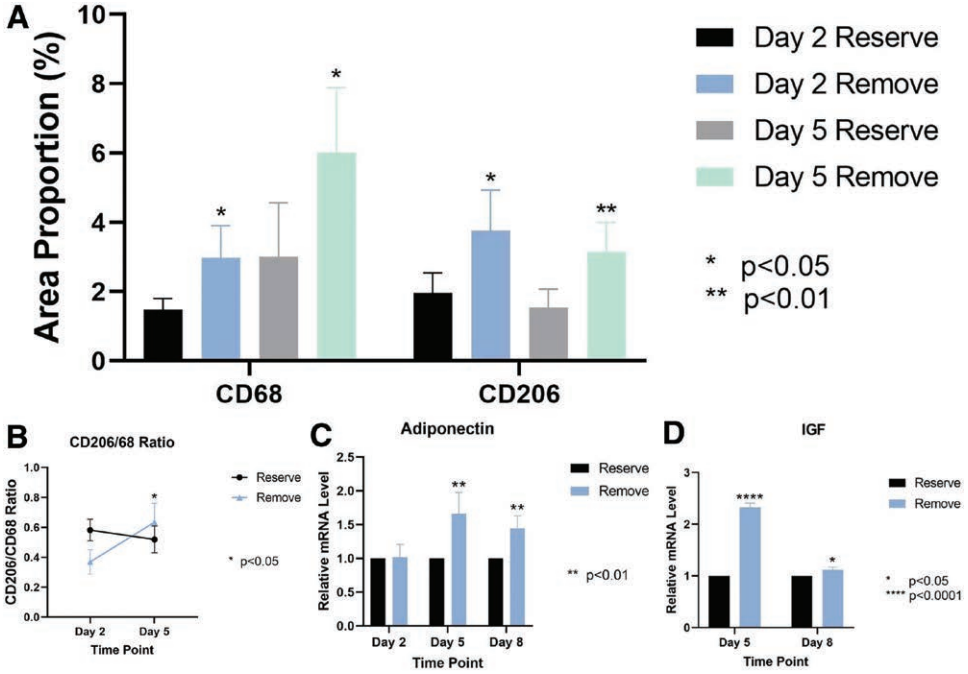

Fig. 4. Reserving eschar declined the level of total macrophages and M2 macrophages in wounds. CD68/CD206 IHC staining of the preserved group and removal group was performed on days 2 and 5, and the infiltration and proportion of M2 macrophages were calculated (A, B). The mRNA levels of adiponectin and IGF were detected by RT-PCR (C, D). Data are presented as mean ± S.D.; **P* < 0.05, ***P* < 0.01, as compared with the reserve group each day. IHC, immunohistochemistry; RT-PCR, reverse transcription-polymerase chain reaction.

on day 5 (n = 12, 0.57 ± 0.15 times, $P < 0.01$). (**See figure, Supplemental Digital Content 7,** which demonstrates IHC staining of macrophages in the removal and the preserved group. **http://links.lww.com/GOX/A6**.)

Reserving Eschar Prevented M2 Macrophages Polarization

CD68/206 HIC staining declared that total macrophage levels elevated over time in the two groups, whereas M2 macrophage numbers diminished (Fig. 4a). The infiltration level of total macrophages (n = 12, 1.49 ± 0.32% versus 3.65 ± 0.87%, $P < 0.05$) and M2 macrophages (n = 12, 1.97 ± 0.51% versus 3.76 ± 1.05%, $P < 0.05$) in the preserved group were both consistently lower than that in the removal group on day 2. It was the same on day 5, showing a lower level of total macrophages (n = 12, 2.98 ± 0.83% versus 6.02 ± 1.67%, $P < 0.05$) and M2 macrophages (n = 12, 1.55 ± 0.47% versus 3.15 ± 0.76%, $P < 0.01$). In particular, the proportion of M2 macrophages in total macrophages downregulated on day 5, which manifested that reserving eschar inhibited the level of M2 macrophages (n = 12, $P < 0.05$, Fig. 4B). Meanwhile, the expression levels of cytokines including adiponectin (n = 12, $P < 0.05$, Fig. 4C) and insulin-like growth factors (IGF) (n = 12, $P < 0.05$, $P < 0.0001$, Fig. 4D) associated with M2 macrophages were synchronously suppressed.

M2 Macrophages Promoted Migration, Proliferation, and Protein Expression of Myofibroblasts

As shown in the scratch assay, co-culture with M2 macrophages enhanced the migration of myofibroblasts compared with the control treatment at 0 hours (n = 12, $P < 0.01$), 12 hours (n = 12, $P < 0.01$), and 24 hours (n = 12, $P < 0.001$) after the scratch (Fig. 5A). (**See figure, Supplemental Digital Content 8,** which demonstrates images of scratch tests on myofibroblasts in the control group and co-culture group. **http://links.lww.com/GOX/A7**) (**See figure, Supplemental Digital Content 9,** which demonstrates the identification of polarized M2 macrophages induced by multiple stimuli in vitro with flow cytometry. **http://links.lww.com/GOX/A8**) Similarly, the proliferation of myofibroblasts in the 24 hour-supernatant group of M2 macrophages was significantly increased after 24 hour and 48 hour culture (n = 12, $P < 0.05$, Fig. 5B).

The morphology of myofibroblasts became longer and more slender after co-culture for 24 hours (Fig. 5E, F). The expression level of α-SMA in the whole 48 hours (Fig. 5C) and the mRNA level of vimentin at 24 hours (n = 12, 1.41 ± 0.10 times, $P < 0.001$, Fig. 5G) in the co-culture group were also significantly higher than those in the control group. Notably, the mRNA level of α-SMA (Fig. 5D) kept a relatively and increasingly higher level in the co-culture environment at 24 hours (n = 12, 1.38 ± 0.13 times, $P < 0.01$) and 48 hours (n = 12, 2.18 ± 0.62 times, $P < 0.05$).

DISCUSSION

compared with severe burns, skin necrosis caused by cosmetic procedures such as laser surgery or facial injections is typically confined to relatively small areas due to

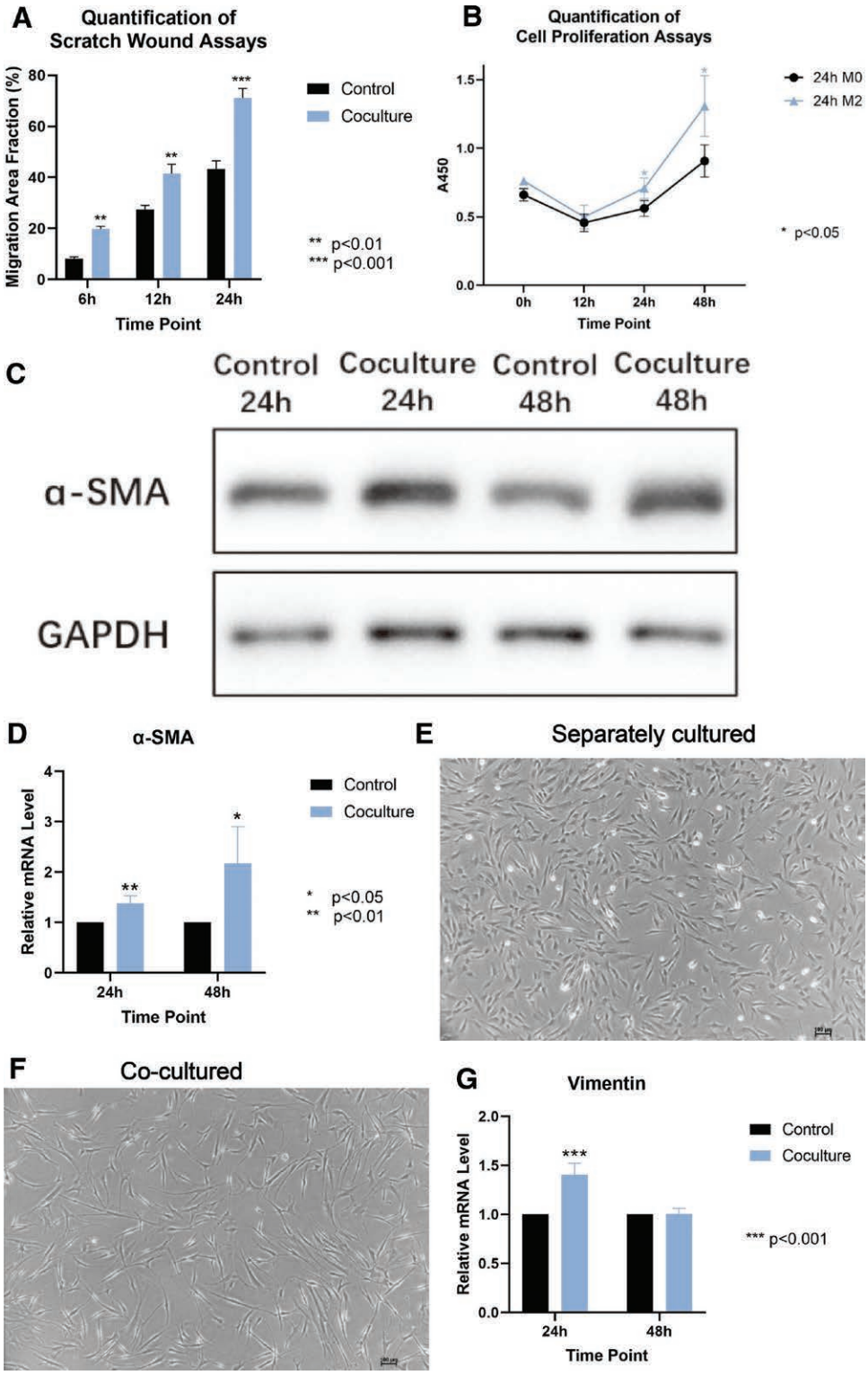

Fig. 5. M2 macrophages promoted the migration, proliferation, and contraction of myofibroblasts. Myofibroblasts induced by HFF-1 cells and M2 macrophages induced by THP-1 cells were co-cultured (E, F). The scratch assay and CCK-8 test were performed (A, B). The expression of α-SMA (C, D) and vimentin (G) were detected by RT-PCR and western bolt. Data are presented as mean ± S.D.; **P* < 0.05, ***P* < 0.01, ****P* < 0.001, as compared with controls for each hour. HFF-1, human foreskin fibroblasts; THP-1, human myeloid leukemia mononuclear cells; CCK-8, counting kit-8; α-SMA, α-smooth muscle actin; RT-PCR, reverse transcription-polymerase chain reaction.

high-energy tissue damage[22] or vascular compression.[23] Studies involving fillers can be simulated using rabbit ear vein injection models,[24,25] with the inability to control the range and extent of skin necrosis to the same degree. In classic burn experiments,[26] the electric burn model is complex using larger animals to achieve comparable damage observed in humans, whereas burns with hot water often result in extensive skin damage. Therefore, we referred to the most classic and easy electric heating pad to establish a localized burn model in our experiments.

Two aspects mainly influence the aesthetic effect of wound healing: first, excessive wound contraction may cause malunion; second, excessive proliferation of collagen fibres may lead to scar thickening. α-SMA is recognized as a key protein in wound contractility, which can help myofibroblasts connect their own cytoskeleton by adhering to the extracellular matrix (ECM). As one of the cytoskeletal proteins, vimentin can not only maintain mechanically stable structure in the interior but also change arrangement by surface stress of wound.[27,28] Nevertheless, relevant research on vimentin is seldom reported. Recent studies revealed normal wound healing is ensured by a subtle balance of myofibroblast activity.[29] Although the exact time and mechanism of the equilibrium point are not entirely clear,[29] we can be confident that the persistence of myofibroblasts activity after physiological wound healing leads to tissue contraction. Here, we found that the levels of α-SMA and vimentin in the removal group were higher than those in the preserved group at all phases, most significant in the remodeling phase. This confirms that the removal of eschar intensifies myofibroblast transformation and has a strong possibility of wound excess contraction. The percentage of collagen in full-thickness skin demonstrated that collagen descended at first and then rose with debridement and the level overall was higher compared with the preserved group on day 21. The possible reason was that a considerable thickness of the dermis was removed under operation; thus, it was bound to be lower at the initial stage of healing. We speculated that the difference would be more pronounced over time. Taken together, we concluded that reserving eschar could improve the aesthetics of wound healing to some extent by reducing wound contraction and excessive collagen hyperplasia.

Furthermore, elevated levels of multiple inflammatory factors were detected in the removal group, including pro-inflammatory factors (IL-6 and TNF-α) secreted by M1 macrophages and anti-inflammatory factors (IL-10) secreted by M2 macrophages, which were probably triggered by secondary inflammation after the removal of eschar. Interestingly, the changes in the anti-inflammatory factor IL-4 were different. On the second day, the augmented level of IL-4 without eschar was far more than other pro-inflammatory factors. It diminished 5 days after modeling conversely, which might be caused by the antagonism between TNF-α and IL-4. M2 macrophage polarization is notoriously stimulated with IL-4; so, we hypothesized the proportion of M2 macrophages rose in the wound after the early phase of secondary inflammation.

Disturbances in macrophage function contribute to pathological fibrosis and aberrant repair. As pointed out by Pradere et al,[30] myofibroblast survival enhanced by hepatic macrophages caused the development of liver fibrosis, especially in the early stages in healing.[31] The balance and mutual transformation between M1 and M2 macrophages play an important role in wound repair. The lack of conversion from M1-type pro-inflammatory to M2-type anti-inflammatory results in nonhealing,[32] whereas the prolonged and heightened inflammatory response contributes to dysregulated fibrosis. Figure 3 displays a decline in total macrophages in the dermis during inflammatory and proliferative phases in the preserved group with the restraint of the proportion of M2 macrophages. Also, adiponectin and IGF showed a simultaneous reduction in the proliferation and remodeling phases. Adiponectin promotes the activation of human monocytes into anti-inflammatory M2 macrophages,[33] and growth factors IGF-1 are released by M2 macrophages.[34] Downregulation of those M2-related cytokines further verified that retention of eschar inhibited M2 macrophage polarization and effects. Moreover, it is worth emphasizing that both adiponectin and IGF have a theoretical basis for affecting myofibroblasts[35,36] and driving tissue fibrosis,[37,38] indicating that M2 macrophages may influence wound healing through myofibroblasts.

To further probe the relationship between M2 macrophages and myofibroblasts, myofibroblasts were cultivated together with M2 macrophages for 24 hours, and we confirmed that the migration and proliferation of myofibroblasts were more evident with simultaneous augmented levels of α-SMA and vimentin in myofibroblasts, promoting the contractile ability and the adhesion with ECM.[39] The above results present that the surface stress of the wound is probably rising to the upregulation of M2 macrophages. An increase in skin tension probably leads to scar contracture and rigid or stiff tissue.[40] Mechanical and other signals are interdependent during regenerative wound healing, but the mechanism needs further exploration.

Based on our experiments, preserving eschar prevents excessive wound healing after dermal necrosis, which means fewer aesthetic concerns, functional issues, and subjective symptoms like itching and pain.[41] Undeniably, this study had certain limitations. Firstly, due to the stronger infection resistance and healing ability of mice compared with humans,[42] there will inevitably be differences between the research findings and the clinical reality. Secondly, we overlooked certain conditions like infection[43] or presence of implants, and our evaluation of wound healing was not comprehensive without morphological wound analysis[44] and scar assessment.[45] Lastly, it must be acknowledged that our study did not include clinical samples, resulting in limited clinical applicability.[46,47] Further experiments will consider comparing the efficacy of the eschar preservation with other treatment methods in patients, aiming to provide more robust clinical evidence.

CONCLUSIONS

Our study revealed that preservation of eschar could prevent excessive wound contraction and scar formation by decreasing M2 macrophages and myofibroblasts, which offers a theoretical basis for further research and the

clinical strategy for the benefit of better aesthetic wound healing.

Yuyan Pan, MD
Department of Plastic and Reconstructive Surgery
Zhongshan Hospital, Fudan University
180 Fenglin Rd, Shanghai 200032
China
E-mail: pyygrace@163.com

Fazhi Qi, MD
Department of Plastic and Reconstructive Surgery
Zhongshan Hospital, Fudan University
180 Fenglin Rd, Shanghai 200032
China
E-mail: qi.fazhi@zs-hospital.sh.cn

DISCLOSURES

The authors have no financial interest to declare in relation to the content of this article. This study was supported by the National Natural Science Foundation of China (Project No. 82102333).

REFERENCES

1. Zhang LX, Lai LY, Zhou GW, et al. Evaluation of intraarterial thrombolysis in treatment of cosmetic facial filler-related ophthalmic artery occlusion. *Plast Reconstr Surg.* 2020;145:42e–50e.
2. Beauvais D, Ferneini EM. Complications and litigation associated with injectable facial fillers: a cross-sectional study. *J Oral Maxillofac Surg.* 2021;79:1180.
3. Cohen JL. Understanding, avoiding, and managing dermal filler complications. *Dermatol Surg.* 2008;34:S92–S99.
4. Harries RL, Bosanquet DC, Harding KG. Wound bed preparation: TIME for an update. *Int Wound J.* 2016;13(Suppl 3):8–14.
5. Ayaz M, Bahadoran H, Arasteh P, et al. Early excision and grafting versus delayed skin grafting in burns covering less than 15% of total body surface area; a non- randomized clinical trial. *Bull Emerg Trauma.* 2014;2:141–145.
6. Hirche C, Kreken Almeland S, Dheansa B, et al. Eschar removal by bromelain based enzymatic debridement (Nexobrid) in burns: European consensus guidelines update. *Burns.* 2020;46:782–796.
7. Mosier MJ, Gibran NS. Surgical excision of the burn wound. *Clin Plast Surg.* 2009;36:617–625.
8. Ziegler B, Fischer S, Pieper D, et al. Evidence and trends in burn wound debridement: an evidence map. *Plast Surg (Oakv).* 2020;28:232–242.
9. Korting HC, Schöllmann C, White RJ. Management of minor acute cutaneous wounds: importance of wound healing in a moist environment. *J Eur Acad Dermatol Venereol.* 2011;25:130–137.
10. Phan QM, Sinha S, Biernaskie J, et al. Single-cell transcriptomic analysis of small and large wounds reveals the distinct spatial organization of regenerative fibroblasts. *Exp Dermatol.* 2021;30:92–101.
11. Nayfeh T, Shah S, Malandris K, et al. A systematic review supporting the American society for dermatologic surgery guidelines on the prevention and treatment of adverse events of injectable fillers. *Dermatol Surg.* 2021;47:227–234.
12. Monsuur HN, van den Broek LJ, Jhingoerie RL, et al. Burn eschar stimulates fibroblast and adipose mesenchymal stromal cell proliferation and migration but inhibits endothelial cell sprouting. *Int J Mol Sci* . 2017;18:1790.
13. Chinese Burn Association. National expert consensus on the clinical application of eschar dermabrasion in burn wounds (2021 version). *Zhonghua Shao Shang Za Zhi.* 2021;37:501–507. [In Chinese]
14. de Barros M, Coltro PS, Hetem CMC, et al. Revisiting escharotomy in patients with burns in extremities. *J Burn Care Res.* 2017;38:e691–e698.
15. Jeong W, Yang CE, Roh TS, et al. Scar prevention and enhanced wound healing induced by polydeoxyribonucleotide in a rat incisional wound-healing model. *Int J Mol Sci* . 2017;18:1698.
16. Eming SA, Wynn TA, Martin P. Inflammation and metabolism in tissue repair and regeneration. *Science.* 2017;356:1026–1030.
17. Gieseck RL, III, Wilson MS, Wynn TA. Type 2 immunity in tissue repair and fibrosis. *Nat Rev Immunol.* 2018;18:62–76.
18. Lucas T, Waisman A, Ranjan R, et al. Differential roles of macrophages in diverse phases of skin repair. *J Immunol.* 2010;184:3964–3977.
19. Zhang T, Wang XF, Wang ZC, et al. Current potential therapeutic strategies targeting the TGF-β/Smad signaling pathway to attenuate keloid and hypertrophic scar formation. *Biomed Pharmacother.* 2020;129:110287.
20. Wang YY, Jiang H, Pan J, et al. Macrophage-to-myofibroblast transition contributes to interstitial fibrosis in chronic renal allograft injury. *J Am Soc Nephrol.* 2017;28:2053–2067.
21. Wang J, Xu L, Xiang Z, et al. Microcystin-LR ameliorates pulmonary fibrosis via modulating CD206(+) M2-like macrophage polarization. *Cell Death Dis.* 2020;11:136.
22. Alster TS, Li MK. Dermatologic laser side effects and complications: prevention and management. *Am J Clin Dermatol.* 2020;21:711–723.
23. Lee W, Oh W, Oh SM, et al. Comparative effectiveness of different interventions of perivascular hyaluronidase. *Plast Reconstr Surg.* 2020;145:957–964.
24. Moon HJ, Lee W, Kim JS, et al. Aspiration revisited: prospective evaluation of a physiologically pressurized model with animal correlation and broader applicability to filler complications. *Aesthet Surg J.* 2021;41:NP1073–NP1083.
25. Hwang CJ, Morgan PV, Pimentel A, et al. Rethinking the role of nitroglycerin ointment in ischemic vascular filler complications: an animal model with ICG imaging. *Ophthalmic Plast Reconstr Surg.* 2016;32:118–122.
26. Abdullahi A, Amini-Nik S, Jeschke MG. Animal models in burn research. *Cell Mol Life Sci.* 2014;71:3241–3255.
27. Patteson AE, Vahabikashi A, Goldman RD, et al. mechanical and non-mechanical functions of filamentous and non-filamentous vimentin. *Bioessays.* 2020;42:e2000078.
28. Walker JL, Bleaken BM, Romisher AR, et al. In wound repair vimentin mediates the transition of mesenchymal leader cells to a myofibroblast phenotype. *Mol Biol Cell.* 2018;29:1555–1570.
29. Hinz B. The role of myofibroblasts in wound healing. *Curr Res Transl Med.* 2016;64:171–177.
30. Wynn TA, Vannella KM. Macrophages in tissue repair, regeneration, and fibrosis. *Immunity.* 2016;44:450–462.
31. Hesketh M, Sahin KB, West ZE, et al. Macrophage phenotypes regulate scar formation and chronic wound healing. *Int J Mol Sci.* 2017;18:1545.
32. Ganesh GV, Ramkumar KM. Macrophage mediation in normal and diabetic wound healing responses. *Inflamm Res.* 2020;69:347–363.
33. Tilg H, Moschen AR. Adipocytokines: mediators linking adipose tissue, inflammation and immunity. *Nat Rev Immunol.* 2006;6:772–783.
34. Chu SY, Chou CH, Huang HD, et al. Mechanical stretch induces hair regeneration through the alternative activation of macrophages. *Nat Commun.* 2019;10:1524.
35. Marangoni RG, Korman BD, Wei J, et al. Myofibroblasts in murine cutaneous fibrosis originate from adiponectin-positive intradermal progenitors. *Arthritis Rheumatol.* 2015;67:1062–1073.

36. Vannella KM, Wynn TA. Mechanisms of organ injury and repair by macrophages. *Annu Rev Physiol.* 2017;79:593–617.
37. Chung EJ, Kwon S, Reedy JL, et al. IGF-1 receptor signaling regulates Type II pneumocyte senescence and resulting macrophage polarization in lung fibrosis. *Int J Radiat Oncol Biol Phys.* 2021;110:526–538.
38. Jing H, Tang S, Lin S, et al. Adiponectin in renal fibrosis. *Aging (Albany NY).* 2020;12:4660–4672.
39. Rippa AL, Kalabusheva EP, Vorotelyak EA. Regeneration of dermis: scarring and cells involved. *Cells.* 2019;8:607.
40. Harn HI, Ogawa R, Hsu CK, et al. The tension biology of wound healing. *Exp Dermatol.* 2019;28:464–471.
41. Lee HJ, Jang YJ. Recent understandings of biology, prophylaxis and treatment strategies for hypertrophic scars and keloids. *Int J Mol Sci* . 2018;19:711.
42. Zomer HD, Trentin AG. Skin wound healing in humans and mice: challenges in translational research. *J Dermatol Sci.* 2018;90:3–12.
43. Church D, Elsayed S, Reid O, et al. Burn wound infections. *Clin Microbiol Rev.* 2006;19:403–434.
44. Guarro G, Cozzani F, Rossini M, et al. Wounds morphologic assessment: application and reproducibility of a virtual measuring system, pilot study. *Acta Biomed.* 2021;92:e2021227.
45. Verhaegen P, van der Wal MBA, Middelkoop E, et al. Objective scar assessment tools: a clinimetric appraisal. *Plast Reconstr Surg.* 2011;127:1561–1570.
46. Boissiere F, Gandolfi S, Riot S, et al. Flap venous congestion and salvage techniques: a systematic literature review. *Plast Reconstr Surg Glob Open.* 2021;9:e3327.
47. Westley S, Mistry R, Dheansa B. Accuracy of virtual assessment in hand trauma. *JPRAS Open.* 2022;31:92–98.